PAPER

Check for updates

A 3D open-framework iron hydrogenophosphate showing high proton conductance under water and aqua-ammonia vapor†

Hai-rong Zhao,[ab] Yin Jia,[b] Yi Gu,[b] Feng-yun He,[b] Kai-ming Zhang, ⓘ *[c] Zheng-fang Tian[d] and Jian-Lan Liu*[a]

Herein we report the first example of the proton conductivity of an open-framework metal phosphate $(NH_3(CH_2)_3NH_3)_2-[Fe_4(OH)_3(HPO_4)_2(PO_4)_3]\cdot4H_2O$ under aqua-ammonia vapor. Its optimized proton conductivity is 5×10^{-2} S cm^{-1} at 313 K and aqua-ammonium vapor from 1 M NH$_3$·H$_2$O solution. That is approximately two orders of magnitude greater than the maximum value under water vapor (8.0×10^{-4} S cm^{-1} at 317 K and 99% RH). The proton transfer mechanism has been proposed in terms of the structural analyses, activation energy calculations, and PXRD determinations.

Open-framework metal phosphates, as a popular kind of porous material, have been widely explored for their potential applications in catalysis, gas separation and magnetism.[1–4] Recently, proton-conductive of open-framework metal phosphates have been becoming an emerging area in the field of fuel cells, in virtue of their porous structure, good proton carriers and hydrogen-bond supported nets, *etc.*[5–11] Similar to metal–organic frameworks (MOFs),[12–18] open-framework metal phosphates have a designable porous structure, in which the channel can provide an efficient path for proton transmission; then usually inorganic metal skeletons are negatively charged, the counter ions in the channels such as NH$_4^+$, enH$_2^+$ are good proton carriers and also help to establish efficient hydrogen-bonding networks for proton hopping or moving. Furthermore, the rigid framework of metal phosphates, which consist of metals and phosphates, endow them with better water and chemical stability than MOFs. Indeed, open-framework metal phosphates have been considered to have important application prospects as proton conductors.

High proton conductivity is one of the important properties of proton conductors. Two methods, which can promote proton conductivity of porous solid proton conductors, like MOFs, porous coordination polymers (PCPs)[19,20] and covalent organic

frameworks (COFs),[21–24] have been well documented, including (1) through modifying the pores of the framework with functional groups (–SO$_3$H, –COOH, *etc.*);[25–27] (2) through introducing proton conducting chemicals or proton carriers into the pores or layers of these materials[16] and (3) through varying the proton conduction environment (such as temperature, relative humidity (RH) and the vapor environment). For example, Luo[28] and coauthors doped imidazole into the pores of the MOF-808, raising the proton conductivity of MOF-808 to 3.45×10^{-2} S cm^{-1} at 338 K and 99% RH. We introduced Na$^+$ ions into the inter-layer of a two-dimensional layered inorganic–organic hybrid metal hydrogenophosphate $(C_2H_{10}N_2)[Mn_2(PO_4)_2]\cdot2H_2O$ *via* ion exchange method. The Na$^+$ ions sharply improve the amount of water sorption of $(C_2H_{10}N_2)[Mn_2(PO_4)_2]\cdot2H_2O$, and promote the formation of a dense and extensive hydrogen-bonding network with water molecules, thus the proton conductivity of the ion exchange product rises to 10^{-2} S cm^{-1} at 283 K and 99% RH.[29] That was more than 900 times higher than $(C_2H_{10}N_2)[Mn_2(PO_4)_2]\cdot2H_2O$ under the same conditions. In addition, the role of water molecule is the key to achieve high proton conductivity for water-mediated proton-conducting materials; therefore, adjusting RH is a common method to vary the proton conductivity. In general, it is found that proton conductivity increases with the rising of RH. In particular, ammonia has a molecular system most similar to that of water, specifically three proton donor sites and one acceptor site with a tetrahedral geometry, a small molecular size (kinetic diameter 2.60 Å) and a degenerate conjugate acid–base system (NH$_4^+$ + NH$_3$ ↔ NH$_3$ + NH$_4^+$).[30,31] Therefrom, we can speculate that ammonia may be a nest promising proton conducting medium. Very recently, Li[32,33] group reported the proton conductivity of two isostructural 3D Co(II) MOFs under aqua-ammonia vapor, both displays that the proton conductivities under aqua-

[a]State Key Laboratory of Materials-Oriented Chemical Engineering, College of Chemistry and Molecular Engineering, Nanjing Tech University, Nanjing 210009, P. R. China. E-mail: njutljl@163.com

[b]School of Environmental Science, Nanjing Xiaozhuang University, Nanjing 210009, P. R. China

[c]Department of Material Engineering, Nanjing Institute of Technology, Nanjing 211167, P. R. China. E-mail: cggzkm@163.com

[d]Hubei Key Laboratory for Processing and Application of Catalytic Materials, Huanggang Normal University, Huanggang 438000, P. R. China

ammonia vapor are significantly enhanced than those under water vapor. This exciting result inspires us to study the open-framework metal phosphates in similar situations to explore the methods to improve the conductivity.

Herein we synthesized a three-dimension metal phosphate $(NH_3(CH_2)_3NH_3)_2–[Fe_4(OH)_3(HPO_4)_2(PO_4)_3]\cdot 4H_2O$ (**1**),[34] and investigated its proton conductivity under water and aqua-ammonia vapor. Our investigation shows that **1** exhibit high proton conductivity in water vapor; then in the aqua-ammonium vapor, proton conductivity sharply increased and reached 5×10^{-2} S cm^{-1} (at 313 K and under aqua-ammonium vapor from 1 M NH$_3\cdot$H$_2$O solution).

Compound **1** crystallizes in the tetragonal space group $I4_1/a$, its asymmetric unit contains two crystallographically independent Fe ions (labeled as Fe(1) and Fe(2)), one HPO$_4^{2-}$ ion (labeled as P(1)), two different PO$_4^{3-}$ ions (labeled as P(2) and P(3)), four coordination water molecules (labeled as O(13), O(14), O(15) and O(16)) and together with two protonated diction of propylenediammonium.

As shown in Fig. 1a, two Fe atoms (Fe(1) and Fe(2)) are both coordinated with six oxygen atoms to form FeO$_6$ octahedra, respectively. Fe(1) is hexacoordinated by three oxygen atoms from PO$_4^{3-}$ anions, one oxygen atoms from HPO$_4^{2-}$ anions and another two bridging oxygen atoms from OH$^-$. Different with that, Fe(2) is ligated by two oxygen atoms from PO$_4^{3-}$ anions, two oxygen atoms from HPO$_4^{2-}$ anions and the rest two

bridging oxygen atoms from OH$^-$. The connectivity of the three PO$_4^{3-}$ tetrahedral are shown in Fig. 1b. For HPO$_4^{2-}$ (P1) and PO$_4^{3-}$ (P2), three oxygen atoms connected with three Fe^{2+}, respectively, and the rest oxygen atoms naked; while for PO$_4^{3-}$ (P3), all oxygen atoms are connected with Fe^{2+}.

Two crystallographically different Fe(2)O$_6$ edge-sharing octahedral into a dimmer and it further linked with two Fe(1)O$_6$ octahedral into a Fe$_4$O$_{20}$ cluster unit (Fig. 1a). Along the a-axis, the Fe$_4$O$_{20}$ cluster unit form an infinite chain via –Fe(1)–O(12)–Fe(1)– bonds with the neighboring two tetramers (Fig. 1c); the chains are interlinked with each other via phosphate tetrahedral to generate a three-dimensional framework structure with large tunnels parallel to (1 0 0) and the diprotonated 1,3-diaminopropane and water molecules order arranged in the channel along the a-axis (Fig. 1d).

As indicated in Fig. 2, 1,3-diaminopropane and water molecules located at the channel via hydrogen bonding interaction. Water molecules are assembled into an infinite chain parallel to a-axis in the sequence O15W–O16W –O16W–O15W–O14W–O13W–O13W–O14W and with O···O distances vary from 2.448 to 2.580 Å, which are much shorter than 2.850 Å in liquid water. Then, the short O···N distances with dO(14)···N(2) = 2.558 Å exist in the 1,3-diaminopropane and water molecules, and dN(1)···O(1) = 2.840 Å, dN(1)···O(2) = 2.964 Å, dN(1)···O(3) = 2.918 Å, dN(1)···O(6) = 2.931 Å, dN(1)···O(8) = 3.044 Å and dN(2)···O(10) = 2.763 Å between 1,3-diaminopropane and the
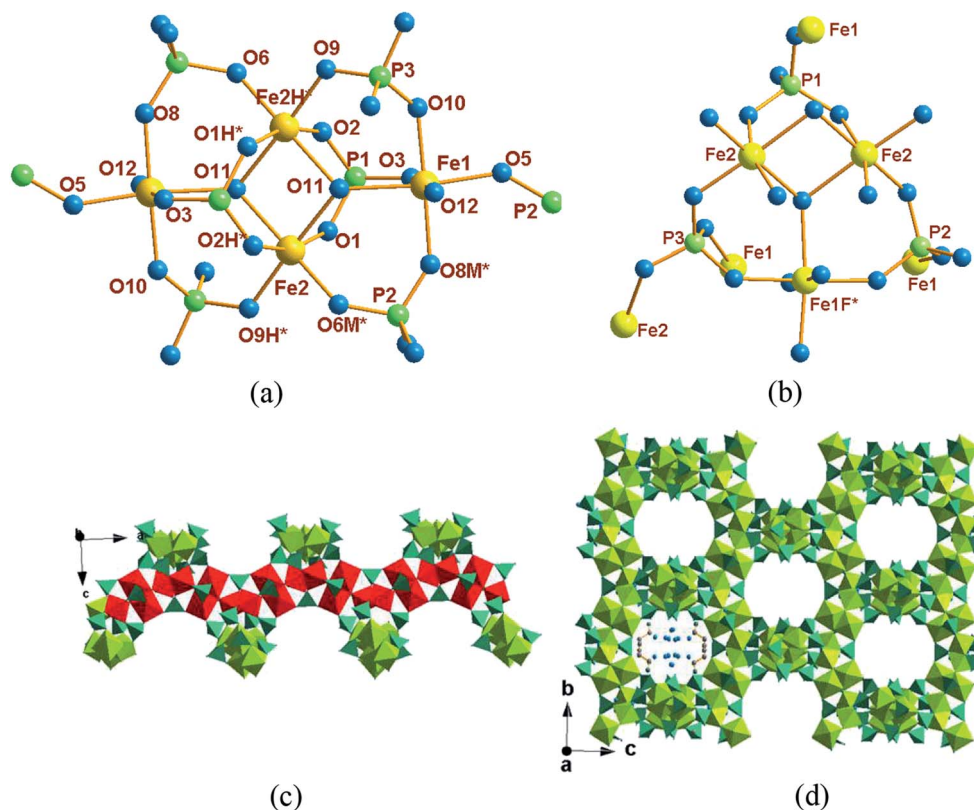
Fig. 1 (a) The Fe$_4$O$_{20}$ cluster unit with the symmetric codes: H* = 1 − x, 2 − y, z; M* = 1 − x, 1.5 − y, 0.25 − z; (b) the connectivity of three HPO$_4^{2-}$ anions; (c) polyhedral representation for a single chain structure constructed by PO$_4^{3-}$ and Fe^{3+}; (d) polyhedral view of the structure of **1** along the a axis.
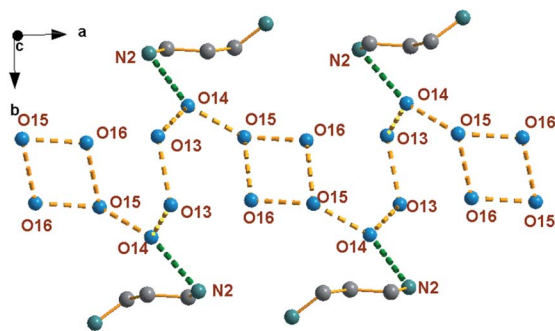
Fig. 2 Hydrogen-bonding interactions in water molecules and between water and ammonia molecules.

inorganic framework. Such highly ordered infinite water chains and strong hydrogen bonding interaction between 1,3-diaminopropane and inorganic framework are the potential proton conducting pathway.

Fig. S1† shows the PXRD profiles of **1** and its sample after exposure in water solution for a month, together with the simulated PXRD pattern of **1**. All of the profiles show high similarity, which indicates that **1** has ultrastrong storage stability. TG and DTA curves of **1** are displayed in Fig. S2.† Three-step decomposition process appeared in the TG curves. The first decomposition step in the range of 298–400 K exhibited 8.3% weight loss, which is close to the calculated value (7.96%) that corresponds to the loss of crystal water in **1**. This weight-losing process is demonstrated in the DTA plot of **1**, in which a peak temperature at 380 K is associated with this process. The second decomposition process starting at 400 K can be attributed to the loss of –OH groups in the inorganic framework. The rest decomposition step that started at 503 K corresponds to the decomposition of charge-compensating cations. The TG and DTA results demonstrated that **1** is thermally stable below *ca.* 500 K.

The temperature dependence of PXRD profiles are shown in Fig. S3.† The PXRD patterns below 423 K are almost the same as 303 K, indicating that the structure of **1** is stable although the water molecules in **1** had lost in the temperature range of 303–400 K. As the temperature further rises to 453 K, the PXRD profiles come to slight change, the diffraction peak of (2 0 0) planes slightly shift toward to higher 2θ degree indicating that the loss of the water molecules in the framework reduces the layer distance. When the temperature reached 513 K, the framework of **1** began to collapse with the strongest diffraction peak of (1 0 1) disappeared. The PXRD datas are consistence with TG that the structure is stable before 500 K.

The ac impedance of powdered sample of **1** under different RH and temperature was carried out. Notably, as shown in Fig. S4,† the proton conductivity of compound **1** is so low (7.3 × 10^{-12} S cm^{-1} at 403 K and 3.1 × 10^{-10} S cm^{-1} at 503 K) under anhydrous condition that it can be ignored. However, after the compound **1** was equilibrated at various relative humidity for 72 h, they exhibit stable conductivity values. To clarify the effect of RH on proton conductivity, the humidity-dependent Nyquist plots of the proton conductivity at 303 K and in the RH range of

60% to 99% were measured. The resultant Nyquist plots are displayed in Fig. S5.† It is to be pointed out that **1** shows unregular semi-circle in the high frequency at low humidity. Nevertheless, at high humidity, the unregular arc in the high frequency and a spike in the low frequency range were observed corresponding to the boundary resistance and a electrode contribution, respectively. Proton conductivity was calculated by fitting the Nyquist plots with the Z-View program. The calculated conductivities, shown in Fig. 3, vary from 2.1 × 10^{-9} S cm^{-1} (60% RH) to 1.62 × 10^{-8} S cm^{-1} (75% RH), and reach a maximum value of 4 × 10^{-4} S cm^{-1} (99% RH). The results indicate that the proton conductivity of **1** is humidity-independent and the conductivity value increases with increasing RH, which may be attribute to the increasing amount of water molecules at high humidity can form more H-bonds with **1**, and promote the transport of protons, increasing the conductivity.

We further measured the Nyquist curves at fixed humidity (99% RH) and varied temperature range of 287 K and 317 K (Fig. 4). The resultant resistance of **1** decreased with elevating temperature, indicating that proton conductivity increased as the rising of temperature. For example, the proton conductivity of **1** is 2.0 × 10^{-4} S cm^{-1} at 287 K, while with the temperature was raised to 317 K, the proton conductivity increased to 8.0 × 10^{-4} S cm^{-1}, which is comparable to some recently reported MOFs, such as Zn-(m-H$_6$L) 1.39 × 10^{-4} S cm^{-1} (at 314 K and 98% RH),[35] PA@Tp-Azo 9.9 × 10^{-4} S cm^{-1} (at 332 K and 98% RH).[36]

Fig. 5 gives the plot of $\ln(\sigma T)$ against 1000/T at 99% RH. The activation energies (E_a) for proton conduction of **1** were calculated by fitting the curve with Arrhenius equation.

$$\ln(\sigma T) = \ln A - \frac{E_a}{k_B T}$$

In equation, the symbol σ represents the proton conductivity, E_a is the proton transport activation energy, k_B is the Boltzmann constant, and A is the pre-exponential factor. The calculated E_a value is 0.32 eV indicating that **1** follow the Grotthuss mechanism, which may that the formation of hydrogen bonding for the immersion of water molecules into the pores
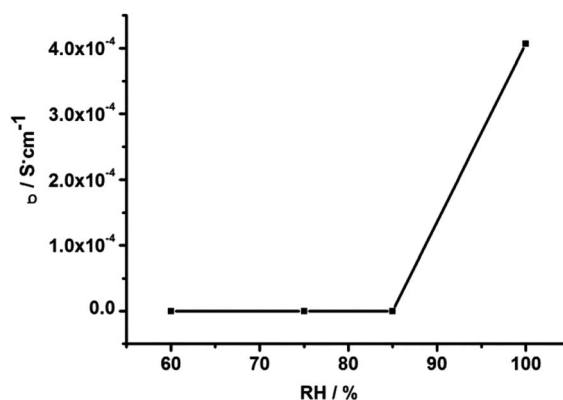

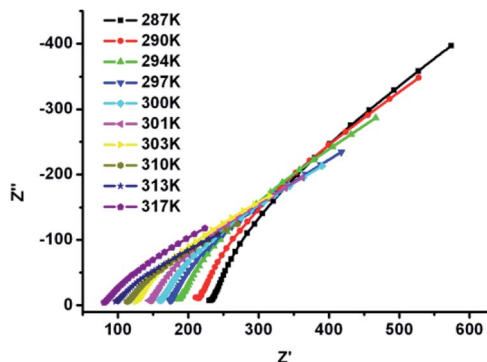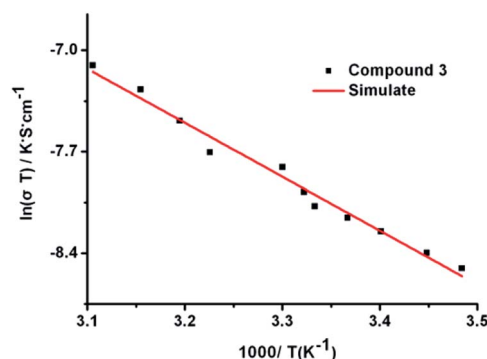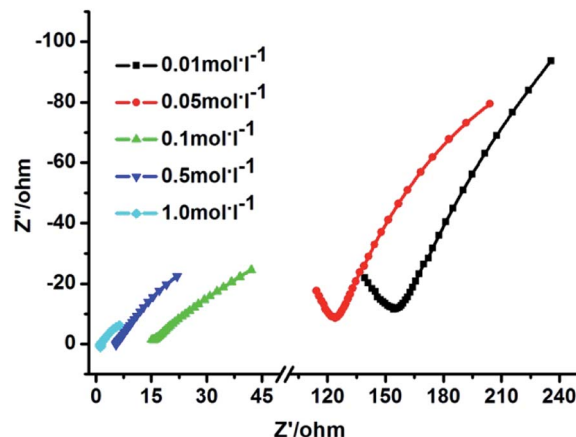Fig. 3 Plots of σ vs. RH at 303 K for compound **1**.

Fig. 4   Nyquist plots of compound **1** at 99% RH.

Fig. 5   The corresponding conductivity in the form of $\ln(\sigma T)$ vs. $1000/T$ for **1**.

Fig. 6   Nyquist plots of compound **1** at different concentration of $NH_3 \cdot H_2O$ solution.

are favorable to proton hopping. Besides that, samples used for proton conductivity testing under water vapor of **1** were determined by PXRD. As shown in Fig. S1,† the PXRD peaks are similar with as-synthesized and simulated data, which demonstrates that the structure of **1** keeps robust after ac impedance determination under water vapor condition.

Based on the above descriptions, we should notice that the optimization proton conductivity of **1** (8.0×10^{-4} S cm^{-1} at 99% RH and 317 K) is apparently smaller than the Nafion-based proton-conducting material ($\sigma = 10^{-1}$ to 10^{-2} S cm^{-1}), which is the unique proton conductive material for industrial application at present, and its proton conductivity is recognized as a benchmark for transcendence. Inspired by some recent research results and the summarized methods to improve the proton conductivity of porous solids, we hope to vary the vapor environment for obtaining high proton conductivity. Specially, we attempted to improve the proton conductivity of **1** by changing the pure water vapor into aqua-ammonia vapor.

The proton conductivity of **1** under aqua-ammonia vapor, obtained from $NH_3 \cdot H_2O$ solutions, was performed by the ac impedance method. Fig. 6 gives the impedance spectra for **1** at 303 K and different aqua-ammonia vapors from 0.01 to 1 M of $NH_3 \cdot H_2O$. The conductivity, calculated by fitting the Nyquist plots with Z-View program, increased from 3.6×10^{-4} S cm^{-1} (0.01 M) to 4.5×10^{-2} S cm^{-1} (1 M), indicating two orders of magnitude increase with the increasing concentration of

$NH_3 \cdot H_2O$ solution. Not only that, the proton conductivity of **1** also showed temperature depended, and the resultant proton conductivity increased with elevating temperature.

For example, the proton conductivity is 2.2×10^{-3} S cm^{-1} at 283 K and it increases to 6.5×10^{-3} S cm^{-1} at 313 K with 0.1 M $NH_3 \cdot H_2O$ solution; the proton conductivity increased from 2.3×10^{-2} S cm^{-1} (283 K) to 5.0×10^{-2} S cm^{-1} (313 K) with 1 M $NH_3 \cdot H_2O$ solution (Fig. S6, Table S1†). These results demonstrated that both high temperature and high concentration aqua-ammonia vapor can promote the improvement of proton conductivity. The maximum proton conductivity value of **1** (5.0×10^{-2} S cm^{-1}) is comparable to that of Nafion and has exceed some reported MOFs under aqua-ammonia vapor and several MOFs containing NH_3 or NH_4^+ components, such as $\{[Co_3(\text{-}DMPhIDC)_2(H_2O)_6] \cdot 2H_2O\}_n$ (4.11×10^{-3} S cm^{-1} at 373 K with 1.5 M $NH_3 \cdot H_2O$ solution), $\{[Co_3(m\text{-}BrPhIDC)_2(H_2O)_6] \cdot 2H_2O\}$ (5.07×10^{-4} S cm^{-1} at 373 K with 1.5 M $NH_3 \cdot H_2O$ solution),[33] Ca-PiPhtA-NH$_3$ (6.6×10^{-3} S cm^{-1} at 297 K and 98% RH).[37]

It also should be noted that, even with relatively low concentration $NH_3 \cdot H_2O$ solution (0.1 M to 0.5 M), the proton conductivity values can be promoted. For instance, the proton conductivity is 6.5×10^{-3} S cm^{-1} at 313 K with 0.1 M $NH_3 \cdot H_2O$ solution and it is 1.3×10^{-2} S cm^{-1} at 313 K with 0.5 M $NH_3 \cdot H_2O$ solution. That is approximately one order and two orders of magnitude greater than the proton conductivity of **1** at 317 K and 99% RH.

The activation energy of **1** under aqua-ammonia vapor was estimated by using the Arrhenius equation to fit its Nyquist plots. The E_a values are listed in Table S1,† and indicating that $E_a > 0.4$ eV while the $NH_3 \cdot H_2O$ solution is less than 0.1 M versus $E_a < 0.4$ eV as the $NH_3 \cdot H_2O$ solution in the range of 0.5 M and 1 M. These results imply that the proton transfer in **1** follows an efficient Grotthuss mechanism with higher concentration of $NH_3 \cdot H_2O$ solution, while the vehicle mechanism is under lower concentration of $NH_3 \cdot H_2O$ solution. This may that higher concentration of $NH_3 \cdot H_2O$ solution form more dense hydrogen bonding network and favor to proton hopping; while lower

concentration of $NH_3 \cdot H_2O$ solution form a relatively sparse hydrogen bonding network and favor to proton transport.

In addition, the PXRD patterns of samples of **1** underwent proton conductivity testing under aqua-ammonia vapor were shown in Fig. S1.† The peaks are similar with as-synthesized and simulated data of **1**, demonstrating that the structure of **1** has strong stability. This is one of the important properties as a good proton conductor material in the practical application.

In summary, we successfully prepared a 3D open-framework iron hydrogenophosphate **1** with excellent thermal and chemical stability and explored its proton conduction under water and aqua-ammonia vapor. We found that compound **1** possessed high proton conductivity at room temperature, especially under aqua-ammonia vapor. The corresponding proton-conducting mechanisms under water and aqua-ammonia vapors were discussed according to experimental results. In addition, the excellent structural stability of **1** underwent electrochemical experiment under water and aqua-ammonia vapor was confirmed by PXRD measure, respectively.

Our work provides a new easy-to-execute method to drastically improve the proton conductivity of open-framework metal phosphates.

Conflicts of interest

There are no conflicts to declare.

Acknowledgements

Notes and references

1 S. T. Wilson, B. M. Lok, C. A. Messina, T. R. Cannan and E. M. Flanigen, Aluminophosphate molecular sieves: a new class of microporous crystalline inorganic solids, *J. Am. Chem. Soc.*, 1982, **104**, 1146–1147.

2 R. Murugavel, A. Choudhury, M. G. Walawalkar, R. Pothiraja and C. N. R. Rao, Metal Complexes of Organophosphate Esters and Open-Framework Metal Phosphates: Synthesis, Structure, Transformations, and Applications, *Chem. Rev.*, 2008, **108**, 3549–3655.

3 M. Moliner, C. Martínez and A. Corma, Synthesis Strategies for Preparing Useful Small Pore Zeolites and Zeotypes for Gas Separations and Catalysis, *Chem. Mater.*, 2014, **26**, 246–258.

4 Y. Li and J. H. Yu, New Stories of Zeolite Structures: Their Descriptions, Determinations, Predictions, and Evaluations, *Chem. Rev.*, 2014, **114**, 7268–7316.

5 Y. Mu, Y. Y. Wang, Y. Li, J. Y. Li and J. H. Yu, Organotemplate-free synthesis of an open-framework magnesium aluminophosphate with proton conduction properties, *Chem. Commun.*, 2015, **51**, 2149–2151.

6 J. Zhu, Y. Yan, J. Liu and X. Song, Synthesis and proton conductivity of a new two-dimensional layered aluminophosphate $[C_9H_{14}N]_8[H_2O]_4 \cdot [Al_8P_{12}O_{48}H_4]$, *Inorg. Chem. Commun.*, 2015, **56**, 133–136.

7 M. Wang, H. B. Luo, S. X. Liu, Y. Zou, Z. F. Tian, L. Li, J. L. Liu and X. M. Ren, Water assisted high proton conductance in a highly thermally stable and superior water-stable open-framework cobalt phosphate, *Dalton Trans.*, 2016, **45**, 19466–19472.

8 R. M. P. Colodrero, K. E. Papathanasiou, N. Stavgianoudaki, P. Olivera-Pastor, E. R. Losilla, M. A. G. Aranda, L. Lón-Reina, J. Sanz, I. Sobrados, D. Choquesillo-Lazarte, J. M. García-Ruiz, P. Atienzar, F. Rey, K. D. Demadis and A. Cabeza, Multifunctional Luminescent and Proton-Conducting Lanthanide Carboxyphosphonate Open-Framework Hybrids Exhibiting Crystalline-to-Amorphous-to-Crystalline Transformations, *Chem. Mater.*, 2012, **24**, 3780–3792.

9 S. Horike, D. Umeyama, M. Inukai, T. Itakura and S. Kitagawa, Coordination-Network-Based Ionic Plastic Crystal for Anhydrous Proton Conductivity, *J. Am. Chem. Soc.*, 2012, **134**, 7612–7615.

10 M. Inukai, T. Itakura and S. Kitagawa, Inherent Proton Conduction in a 2D Coordination Framework, *J. Am. Chem. Soc.*, 2012, **134**, 12780–12785.

11 S. Horike, W. Q. Chen, T. Itakura, M. Inukai, D. Umeyama, H. Asakurae and S. Kitagawa, Order-to-disorder structural transformation of a coordination polymer and its influence on proton conduction, *Chem. Commun.*, 2014, **50**, 10241–10243.

12 Y. S. Wei, X. P. Hu, Z. Han, X. Y. Dong, S. Q. Zang and T. C. W. Mak, Unique Proton Dynamics in an Efficient MOF-Based Proton Conductor, *J. Am. Chem. Soc.*, 2017, **139**, 3505–3512.

13 S.-S. Bao, G. K. H. Shimizu and L. M. Zheng, Proton Conductive Metal Phosphonate Frameworks, *Coord. Chem. Rev.*, 2019, **378**, 577–594.

14 X. Meng, H. N. Wang, S. Y. Song and H. J. Zhang, Proton-Conducting Crystalline Porous Materials, *Chem. Soc. Rev.*, 2017, **46**, 464–480.

15 P. Ramaswamy, N. E. Wong and G. K. Shimizu, MOFs as Proton Conductors-Challenges and Opportunities, *Chem. Soc. Rev.*, 2014, **43**, 5913–5932.

16 F. M. Zhang, L. Z. Dong, J. S. Qin, W. Guan, J. Liu, S. L. Li, M. Lu, Y. Q. Lan, Z. M. Su and H. C. Zhou, Effect of Imidazole Arrangements on Proton-Conductivity in Metal-Organic Frameworks, *J. Am. Chem. Soc.*, 2017, **139**, 6183–6189.

17 M. Inukai, S. Horike, T. Itakura, R. Shinozaki, O. Naoki, D. Umeyama, S. Nagarkar, Y. Nishiyama, M. Malon, A. Hayashi, T. Ohhara, R. Kiyanagi and S. Kitagawa, Encapsulating Mobile Proton Carriers into Structural Defects in Coordination Polymer Crystals: High Anhydrous Proton Conduction and Fuel Cell Application, *J. Am. Chem. Soc.*, 2016, **138**, 8505–8511.

18 X. S. Xing, Z. H. Fu, N. N. Zhang, X. Q. Yu, M. S. Wang and G. C. Guo, High proton conduction in an excellent water-

stable gadolinium metal-organic framework, *Chem. Commun.*, 2019, **55**, 1241–1244.

19 X. L. Su, Z. Z. Yao, Y. X. Ye, H. Zeng, G. Xu, L. Wu, X. L. Ma, Q. H. Chen, L. H. Wang, Z. J. Zhang and S. C. Xiang, 40-Fold Enhanced Intrinsic Proton Conductivity in Coordination Polymers with the Same Proton-Conducting Pathway by Tuning Metal Cation Nodes, *Inorg. Chem.*, 2016, **55**, 983–986.

20 S. Bureekaew, S. Horike, M. Higuchi, M. Mizuno, T. Kawamura, D. Tanaka, N. Yanai and S. Kitagawa, One-dimensional imidazole aggregate in aluminium porous coordination polymers with high proton conductivity, *Nat. Mater.*, 2009, **8**, 831–836.

21 H. Xu, S. Tao and D. Jiang, Proton Conduction in Crystalline and Porous Covalent Organic Frameworks, *Nat. Mater.*, 2016, **15**, 722–726.

22 H. P. Ma, B. L. Liu, B. Li, L. M. Zhang, Y. G. Li, H. Q. Tan, H. Y. Zang and G. S. Zhu, Cationic Covalent Organic Frameworks: A Simple Platform of Anionic Exchange for Porosity Tuning and Proton Conduction, *J. Am. Chem. Soc.*, 2016, **138**, 5897–5903.

23 A. Jankowska, A. Zalewska, A. Skalska, A. Ostrowski and S. Kowalak, Proton Conductivity of Imidazole Entrapped in Microporous Molecular Sieves, *Chem. Commun.*, 2017, **53**, 2475–2478.

24 Y. Ye, L. Zhang, Q. Peng, G. E. Wang, Y. Shen, Z. Li, L. Wang, X. Ma, Q. H. Chen, Z. Zhang and S. Xiang, High Anhydrous Proton Conductivity of Imidazole-Loaded Mesoporous Polyimides Over a Wide Range from Subzero to Moderate Temperature, *J. Am. Chem. Soc.*, 2015, **137**, 913–918.

25 J. Zhang, H. J. Bai, Q. Ren, H. B. Luo, X. M. Ren, Z. F. Tian and S. Lu, Extra Water- and Acid-Stable MOF-801 with High Proton Conductivity and Its Composite Membrane for Proton-Exchange Membrane, *ACS Appl. Mater. Interfaces*, 2018, **10**, 28656–28663.

26 W. J. Phang, H. Jo, W. R. Lee, J. H. Song, K. Yoo, B. Kim and C. S. Hong, Superprotonic conductivity of a UiO-66 framework functionalized with sulfonic acid groups by facile postsynthetic oxidation, *Angew. Chem., Int. Ed.*, 2015, **54**, 5142–5146.

27 P. Ramaswamy, R. Matsuda, W. Kosaka, G. Akiyama, H. J. Jeon and S. Kitagawa, Highly proton conductive nanoporous coordination polymers with sulfonic acid groups on the pore surface, *Chem. Commun.*, 2014, **50**, 1144–1146.

28 H. B. Luo, Q. Ren, P. Wang, J. Zhang, L. F. Wang and X. M. Ren, High Proton Conductivity Achieved by

Encapsulation of Imidazole Molecules into Proton-Conducting MOF-808, *ACS Appl. Mater. Interfaces*, 2019, **11**, 9164–9171.

29 K. M. Zhang, F. Y. He, H. B. Duan and H. R. Zhao, An Alkali Metal Ion-Exchanged Metal-Phosphate $(C_2H_{10}N_2)_xNa_{1-x}[Mn_2(PO_4)_2]$ with High Proton Conductivity of 10^{-2} S cm^{-1}, *Inorg. Chem.*, 2019, **58**, 6639–6646.

30 K. M. Guo, L. L. Zhao, S. H. Yu, W. Y. Zhou, Z. F. Li and G. Li, A Water-Stable Proton-Conductive Barium(II)-Organic Framework for Ammonia Sensing at High Humidity, *Inorg. Chem.*, 2018, **57**, 7104–7112.

31 W. Y. Chen, J. Wang, L. L. Zhao, W. Dai, Z. F. Li and G. Li, Enhancing proton conductivity of a highly water stable 3D Sr(II) metal-organic framework by exposure to aqua-ammonia vapor, *J. Alloys Compd.*, 2018, **750**, 895–901.

32 D.-W. Lim, M. Sadakiyo and H. Kitagawa, Proton transfer in hydrogen-bonded degenerate systems of water and ammonia in metal–organic frameworks, *Chem. Sci.*, 2019, **10**, 16–33.

33 R. L. Liu, L. L. Zhao, W. Dai, C. L. Yang, X. Liang and G. Li, A Comparative Investigation of Proton Conductivities for Two Metal-Organic Frameworks under Water and Aqua-Ammonia Vapors, *Inorg. Chem.*, 2018, **57**, 1474–1482.

34 K. H. Lii and Y. F. Huang, Large tunnels in the hydrothermally synthesized open-framework iron phosphate $[H_3N(CH_2)_3NH_3]_2[Fe_4(OH)_3(HPO_4)_2 - (PO_4)_3]\cdot xH_2O$, *Chem. Commun.*, 1997, 839–840.

35 R. M. P. Colodrero, G. K. Angeli, M. Bazaga-Garcia, P. Olivera-Pastor, D. Villemin, E. R. Losilla, E. Q. Martos, G. B. Hix, M. A. G. Aranda, K. D. Demadis and A. Cabeza, Structural Variability in Multifunctional Metal Xylenediaminetetraphosphonate Hybrids, *Inorg. Chem.*, 2013, **52**, 8770–8783.

36 S. Chandra, T. Kundu, S. Kandambeth, R. BabaRao, Y. Marathe, S. M. Kunjir and R. Banerjee, Phosphoric Acid Loaded Azo (−N=N−) Based Covalent Organic Framework for Proton Conduction, *J. Am. Chem. Soc.*, 2014, **136**, 6570–6573.

37 M. Bazaga-García, R. M. Colodrero, M. Papadaki, P. Garczarek, J. Zon, P. O. Pastor, E. R. Losilla, L. L. Reina, M. A. Aranda, D. C. Lazarte, K. D. Demadis and A. Cabeza, Guest Molecule-Responsive Functional Calcium Phosphonate Frameworks for Tuned Proton Conductivity, *J. Am. Chem. Soc.*, 2014, **136**, 5731–5739.